ADVANCED FUNCTIONAL MATERIALS
www.afm-journal.de

Sustained Antibiotic Release from Biodegradable Gelatin–Silica Hybrid for Orthopedic Infections

Yu-Chien Lin, Chin-Yun Lee, Julian R. Jones, Wai-Ching Liu, Nam-Joon Cho, Chih-Chien Hu,* and Ren-Jei Chung**

Antibiotic-loaded polymethylmethacrylate (PMMA) beads are commonly employed to treat prosthetic joint infections (PJI) and chronic osteomyelitis due to their excellent mechanical strength. However, PMMA's non-degradability results in a burst release of antibiotics and potential renal toxicity, necessitating additional surgeries for bead removal. There is a critical need for infection control materials that can deliver antibiotics effectively, maintain adequate mechanical strength, and degrade uniformly. This study introduces a gelatin–silica hybrid antibiotic carrier, characterized by covalent bonds between the gelatin and silica networks. The incorporation of the silica network enhances the compressive strength to 32.53 ± 2.4 MPa and ensures uniform degradation over 6 months, aligning with clinical timelines. Furthermore, the gelatin–silica hybrid can support up to 10 wt% antibiotic loading without compromising its properties, making it a promising candidate for next-generation infection control materials.

1. Introduction

Orthopedic infection is a highly complex and difficult-to-avoid problem.[1] Although the demand for orthopedic implant surgeries such as total hip arthroplasty and total knee arthroplasty has been increasing, the risk of periprosthetic joint infection (PJI) also rises with factors like patient age and material fatigue.[2] ≈15% of patients develop PJI after hip repair and 25% for knee repairs, with a five-year mortality rate higher than that of breast cancer.[3] Hip arthroplasty revision rates due to deep infections are expected to increase from 8.4% in 2005 to 47.5% by 2030, and for knee arthroplasty repairs, an increase from 16.8% to 65.5% is predicted.[4]

In the conventional treatment for chronic osteomyelitis, a two-stage surgery is performed. First, the implant is removed, and the area is thoroughly cleaned. Then, local antibiotic carriers are placed to treat infections.[5] Therefore, a combination of different antibiotics is necessary to provide comprehensive treatment.[6] Currently, antibiotic-loaded polymethylmethacrylate (PMMA) beads are used clinically to treat PJI and chronic osteomyelitis.[7] Initially, PMMA beads release a burst of antibiotics in the first week, followed by a significant decline in concentration.[8] This burst release can stress the body and potentially cause acute kidney injury, while the prolonged low-level release may lead to drug resistance or biofilm formation.[9] Studies indicate that PMMA beads typically

---

Y.-C. Lin, C.-Y. Lee, R.-J. Chung
Department of Chemical Engineering and Biotechnology
National Taipei University of Technology
Taipei 10608, Taiwan
E-mail: rjchung@mail.ntut.edu.tw

Y.-C. Lin, N.-J. Cho
School of Materials Science and Engineering
Nanyang Technological University
Singapore 639798, Singapore
E-mail: NJCho@ntu.edu.sg

J. R. Jones
Department of Materials
Imperial College London
London SW7 2BP, UK

W.-C. Liu
Department of Food and Health Sciences
Technological and Higher Education Institute of Hong Kong
New Territories
Hong Kong

N.-J. Cho
Centre for Cross Economy Global
Nanyang Technological University
Singapore 637553, Singapore

C.-C. Hu
Bone and Joint Research Center
Chang Gung Memorial Hospital
Linko 333, Taiwan
E-mail: r52906154@cgmh.org.tw

C.-C. Hu
Department of Orthopaedic Surgery
Chang Gung Memorial Hospital
Linko 333, Taiwan

C.-C. Hu
College of Medicine
Chang Gung University
Taoyuan 333, Taiwan

R.-J. Chung
High-Value Biomaterials Research and Commercialization Center
National Taipei University of Technology
Taipei 10608, Taiwan

The ORCID identification number(s) for the author(s) of this article can be found under https://doi.org/10.1002/adfm.202409491

DOI: 10.1002/adfm.202409491

release only ≈5% of their total antibiotic content, limiting precise dosage control and optimal treatment.[10] After the inflammation is cleared, a second surgery is required to remove the PMMA beads and perform subsequent implantation. Local antibiotic delivery is currently a method to improve treatment outcomes and enhance biofilm eradication.[11] Due to the lack of effective long-term antibiotic carriers, patients using PMMA beads still need to take antibiotics orally or via injection for up to 6 weeks.[12] For elderly or diabetic patients, the treatment duration may extend to 8–12 weeks or longer,[13] causing significant medical burdens. To address this, there is a need to develop a material that can provide sustained drug release, fill voids created during debridement, and promote tissue healing as it gradually degrades, eliminating the need for secondary surgery. This carrier should support tissue repair, fill post-debridement voids, and ensure long-term stable antibiotic release.

Here, we have designed a gelatin–silica hybrid material that addresses the aforementioned requirements. From our previous research,[14] it can be inferred that by altering the ratio of (3-Glycidyloxypropyl)trimethoxysilane (GPTMS) coupling agent to gelatin, there can be an increase in inorganic-organic coupling. This results in the provision of a covalent link from the organic gelatin molecules to the inorganic silicate network, forming covalent bonds at the molecular scale.[15] As a result, the material exhibits the characteristics of organic compounds such as drug-loading capability, moldability, and biodegradability.[16] The inorganic component provides overall material strength, slows degradation, and generates numerous active sites of Si—OH during the hydrolysis process of silica. These active sites can supply metal ions (e.g., calcium, phosphate ions) required for new bone formation, promoting the repair of surrounding bone tissue.[17] Additionally, degradation of silica networks releases silica species which can stimulate collagen and new blood vessel formation.[18] Complete material degradation enables precise dosage during drug administration, with adjustable drug release and degradation rates achieved by modulating the composition ratio. These rates can range from hours to months, alongside customizable mechanical properties. Moreover, the gelatin–silica hybrid material allows antibiotic mixing within ≈15–20 min without generating any exothermic reactions. It can be shaped through molding, injection, or manual techniques. The advancement of this material offers promise in enhancing the effectiveness of antibiotic carriers for PJI applications.

2. Results and Discussion

2.1. Chemical and Composition Characterizations

Gelatin-silica hybrids and drug-loaded gelatin–silica hybrids were synthesized by incorporating GPTMS-functionalized gelatin into a sol of hydrolyzed tetraethyl orthosilicate (TEOS), with the drug directly mixed during polymerization.[14] To verify the successful synthesis of both gelatin–silica hybrids and drug-loaded gelatin–silica hybrids, Fourier transform infrared spectroscopy (FTIR) analysis was performed. Figure S1 (Supporting Information) displays the FTIR spectra of 70S/30G (70 wt% silica/30 wt% gelatin), 60S/40G, and 50S/50G. **Figure 1a** displays the FTIR spectra of TEOS, Gelatin, 60S/40G, and 60S/40G-CV (10 wt% CV loaded in 60S/40G, where CV is a 1:1 mixture of C (ceftazidime) and V (vancomycin), totaling 10 wt% load). Hydrolyzed TEOS shows bands at 1059 and 1640 cm^{-1}, corresponding to Si—O—Si stretching and O—H vibration due to water presence.[19] Gelatin features characteristic bands at 666 cm^{-1} (N—H wagging), 1549 cm^{-1} (N—H bending, amide II), 1640 cm^{-1} (C=O stretching, amide I), and 3320 cm^{-1} (N—H stretching).[20] The spectra of 50S/50G, 60S/40G, and 70S/30G show absorption bands at 1549, 1640, and 3320 cm^{-1}, indicating the formation of a gelatin–silica hybrid.[14] The FTIR peaks remained consistent despite increased silica content. For antibiotic-loaded 60S/40G-CV, no additional peaks were observed due to overlapping bands. The gelatin–silica hybrid, covalently bonded via GPTMS, consists of organic gelatin, which has a significantly lower thermal decomposition temperature compared to silica. The organic-to-inorganic ratio can be evaluated using TGA analysis.[14] Figure 1b indicates that pure Gelatin exhibits a 99.8 wt% weight loss, while hybrid materials retain significant weight. For 50S/50G, 60S/40G, and 70S/30G, the remaining inorganic content is 40.15%, 47.72%, and 50.35%, respectively. The slight deviation from nominal values is due to the calculation based on gelatin and silicon (Si), with other organic compounds potentially present.

The chemical structure of the gelatin–silica hybrid is essential for its properties, and ^{1}H nuclear magnetic resonance (NMR) spectroscopy has been used to elucidate this structure before and after coupling[14] and epoxy-amino reactions.[21] Figure 1c shows the chemical structures of GPTMS, hydrolyzed TEOS, and the gelatin–silica hybrid. Covalent bonding between gelatin and silica is facilitated by GPTMS, which has three methoxy groups on one side and an epoxy ring on the other. Notable characteristic peaks are labeled, with the epoxide ring of GPTMS appearing at 2.6 and 2.8 ppm.[22] In an acidic environment, TEOS hydrolyzes and undergoes polymer condensation, forming a Si—O—Si network and Si—OH groups.[23] GPTMS also reacts under very acidic conditions (pH 2), where silanols form and begin to condense, creating a network that reacts with GPTMS to form strong bonds. GPTMS is first added to gelatin, where COOH groups on the gelatin catalyze the opening of the epoxy ring. This leads to the formation of diols in higher oligomers, creating short-chain molecules with a methoxysilane group at the end.[24] This results in a significant decrease in the peaks at 2.6 and 2.8 ppm, indicating the successful opening of the epoxide ring.[25] When hydrolyzed TEOS is introduced into the GPTMS and gelatin solution, the formation of the gelatin–silica hybrid solidifies more rapidly with increasing TEOS. Amine groups on gelatin act as catalysts, accelerating silica condensation to form stable silicon pentavalent species and a robust Si—O—Si network.[26] This confirms the successful synthesis of the gelatin–silica hybrid.

2.2. Material Properties Analysis

The surface morphologies of the hybrids observed using scanning electron microscope (SEM), are shown in **Figure 2**. Samples were freeze-dried before observation. Pure gelatin (Figure 2a) exhibits a porous structure with varying pore sizes. In contrast, gelatin–silica hybrids in Figure 2b–d show continuous surfaces regardless of silica content. This smoothness is due to covalent bonds between gelatin and the silica network, preventing pore formation during freeze-drying. Energy dispersive X-ray (EDX) confirmed the presence of carbon and silicon, with

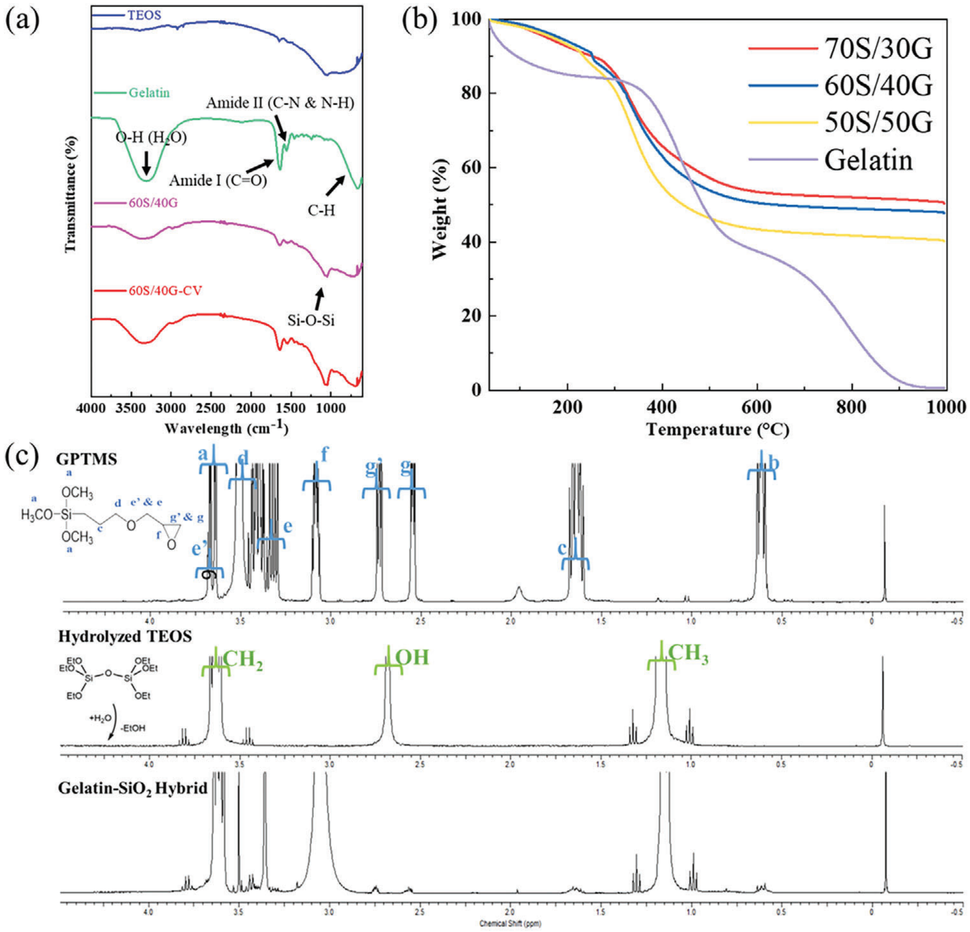

Figure 1. a) FTIR analysis of hydrolyzed TEOS, Gelatin, 60S/40G, and 60S/40G-CV; b) TGA analysis of gelatin–silica hybrids with various silica concentrations; c) ^{1}H NMR spectra of GPTMS, hydrolyzed TEOS, and gelatin–silica hybrid.

homogeneous distribution in all hybrids (Figure S2, Supporting Information). Antibiotic-filled gelatin pores are shown in Figure 2e,m. Cross-sectional images reveal multiple internal fracture patterns in hybrids with high silica content Figure 2j. The 50S/50G samples exhibit creamy scoop structures due to plastic deformation (Figure 2l,p).[27] The 60S/40G samples show a balanced combination of inorganic and organic components without brittle fractures. SEM images demonstrate the homogeneous and continuous structure of the gelatin–silica hybrid compared to porous gelatin.

Figure 3a–c shows the swelling ratio, compressive strength, and Young's modulus of the hybrid, while Figure 3d–f presents these properties in antibiotic-loaded hybrids. Hybrids exhibit sustained swelling over 12 h. The 50S/50G hybrid, with higher gelatin content, swells by 26.81 ± 0.69%, compared to 70S/30G's 16.69 ± 0.35%. Antibiotic-loaded hybrids show reduced swelling, with 50S/50G-CV swelling by 14.33 ± 0.59% and 70S/30G by 5.91 ± 0.72%. Higher silica content forms a compact structure, reducing swelling compared to gelatin-rich hybrids.[28]

Figure 3b,c,e,f, illustrate the mechanical properties of gelatin–silica hybrid materials (50S/50G, 60S/40G, and 70S/30G) with and without antibiotics. The 50S/50G hybrid has the highest stress-strain to failure due to its higher organic content, enhancing strain capacity. The 70S/30G hybrid, with higher silica content, exhibits brittleness and the lowest strain to failure. Young's modulus increases from 101.09 ± 3.57 MPa for 60S/40G to 331.54 ± 16.08 MPa for 70S/30G. Adding antibiotics to 50S/50G significantly decreases compressive strength from 32.53 ± 2.4 MPa to 15.14 ± 1.8 MPa. This reduction is due to the competition for moisture during hybrid synthesis, leading to particle aggregation and creamy scoop structures (Figure 2h,p), weakening structural strength. The 70S/30G composition, lacking sufficient organic gelatin, fails to maintain structural integrity under stress. The 60S/40G hybrid exhibits the most stable mechanical properties, indicating an optimal inorganic-organic blend. Figure 3g, demonstrates the 50S/50G hybrid with a higher proportion of gelatin, hence exhibiting the characteristics of an elastomer. Upon compression, it promptly returns to its original shape.

2.3. Degradation and Drug Release

The properties of the drug carrier are crucial for sustainable antibiotic release. The degradation characteristics of the carrier impact the drug release rate; as the carrier degrades, the drugs are released. Uniform degradation is essential for controlled drug

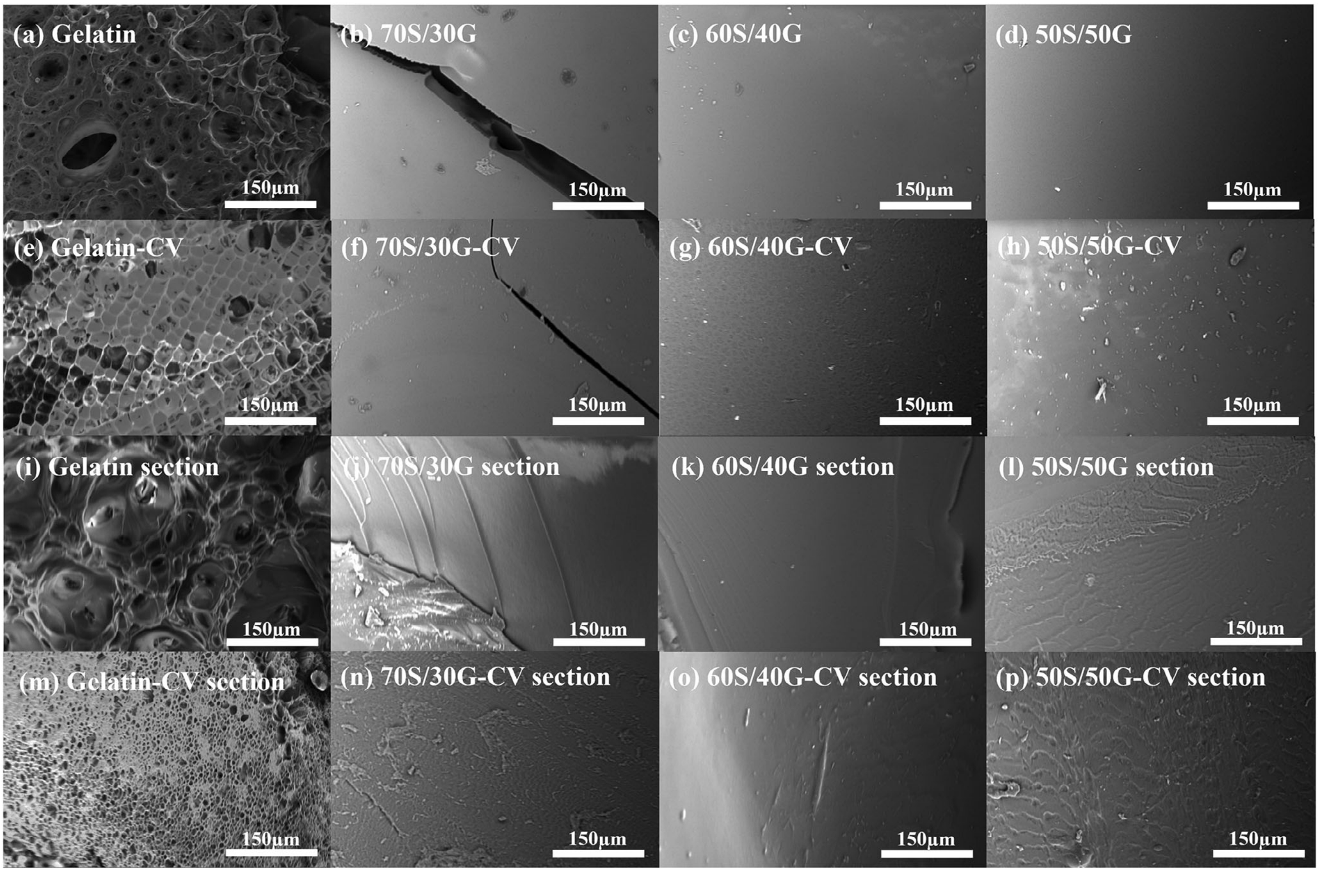

Figure 2. a–h) SEM images show the top view of Gelatin, 70S/30G, 60S/40G, and 50S/50G both with and without antibiotics. i–p) Cross-section SEM images depict Gelatin, 70S/30G, 60S/40G, and 50S/50G with and without antibiotics.

release. Inorganic-organic hybrids are designed to achieve uniform degradation.[29] Traditional composites often have material interfaces that can accelerate localized degradation and result in non-uniform degradation. However, molecular-scale hybrids form stable structures through covalent bonds, ensuring uniform degradation. For example, Tallia et al.[18b] investigated a silica/poly(tetrahydrofuran) (PTHF)/polycarprolactone (PCL)-diCOOH hybrid system, showing that controlled silica content alters mechanical properties. PCL, a biodegradable polymer, exhibited a weight loss of 14.5 ± 0.5 wt% over 7 days without compromising mechanical properties.

Figure 4a,b shows that pure gelatin dissolves completely within 7 days, whereas hybrids degrade slowly and continuously. By 17 weeks, mass loss for 70S/30G, 60S/40G, and 50S/50G was 66.52 ± 2.44%, 84.68 ± 2.07%, and 92.41 ± 1.08%, respectively. Even with antibiotics, mass loss rates were similar. In Figure S3 (Supporting Information), enzyme simulations with 0.5 mg mL^{-1} lysozyme over 9 weeks showed mass loss of 57.97 ± 0.78% (70S/30G), 77.67 ± 1.91% (60S/40G), and 84.68 ± 1.61% (50S/50G). Antibiotic-loaded hybrids showed similar trends. Hybrids with gelatin degrade significantly faster under enzyme action, reducing degradation time from 17 to 9 weeks.[30] In the presence of lysozyme, demonstrating gelatin increases proteolytic degradation, the hybrid can still degrade uniformly over 9 weeks. This is in contrast to previous studies using different crosslinking methods to prepare gelatin-based materials. For example, the Poly(L-lactic acid) (PLLA) and gelatin composite degrades with the gelatin structure collapsing on the first week.[31] Gelatin methacrylate crosslinked using UV radiation[32] and ionically crosslinked gelatin-alginate hydrogel[33] can maintain structural integrity for ≈2 weeks due to the higher crosslinking strength. The gelatin–silica hybrid demonstrates better structural stability compared to other gelatin-based materials.

Figure 4c,d displays cumulative drug release experiments with 10 wt% Ceftazidime or Vancomycin in the hybrid. Pure gelatin degrades in 7 days, with hybrids showing uniform degradation and drug release. Initial 7-day release was ≈19.46 ± 0.71% (70S/30G-C), 20.94 ± 0.25% (60S/40G-C), and 21.37 ± 0.91% (50S/50G-C). For Vancomycin, 24.32 ± 0.51% (70S/30G-V), 24.41 ± 1.11% (60S/40G-V), and 21.41 ± 1.56% (50S/50G-V) were released. This initial burst is likely due to surface-exposed antibiotics. By day 147, drug release reached 78.56 ± 2.71% (70S/30G-C), 84.37 ± 4.44% (60S/40G-C), and 94.70 ± 2.99% (50S/50G-C), with similar results for Vancomycin hybrids.

The experiment demonstrates a crucial correlation between drug release and material degradation. Regardless of enzyme presence, gelatin–silica hybrids exhibit excellent, adjustable degradation characteristics. The degradation experiment involved replacing half of the cocultured medium at each time point until the end of the experiment. Antibacterial testing of the

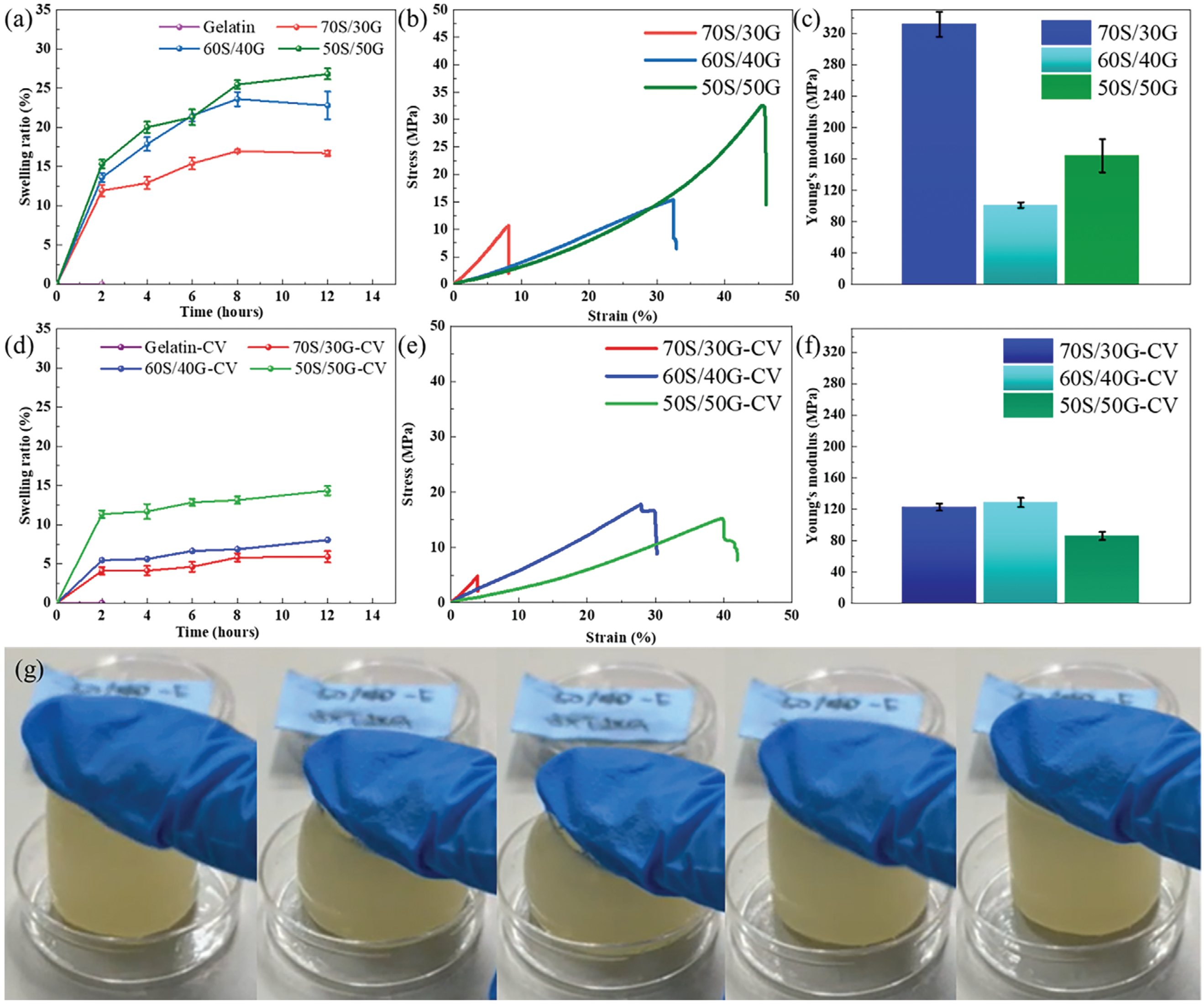

Figure 3. a) Swelling ratio of Gelatin, 70S/30G, 60S/40G, and 50S/50G; b,c) compression test and Young's modulus of 70S/30G, 60S/40G, and 50S/50G; d) swelling ratio of Gelatin, 70S/30G, 60S/40G, and 50S/50G with antibiotics; e,f) compression test and Young's modulus of 70S/30G, 60S/40G, and 50S/50G with antibiotics. g) 50S/50G hybrid was shaped using a 25 mm diameter and 50 mm height Teflon mold and dried at room temperature. The image illustrates, from left to right, the manual compression of the material and its subsequent recovery.

collected medium over 1–5 months showed clear inhibition zones against *Staphylococcus aureus* (*S. aureus*) Figure 4e and *Escherichia coli* (*E. coli*) Figure 4f. Vancomycin was more effective against *S. aureus*, and Ceftazidime against *E. coli*, confirming sustained antibacterial efficacy over five months.

2.4. In Vitro Tests

To confirm the non-toxicity of the material to eukaryotic cells, L929 cells were used to measure the biocompatibility of hybrids containing Ceftazidime or Vancomycin antibiotics, as shown in **Figure 5a,b**. Regardless of the presence of both antibiotics in the hybrid material, cell viability exceeded 90% relative to basal media control. In Figure S4 (Supporting Information), rBMSCs were used to evaluate the biocompatibility of 60S/40G hybrids containing different antibiotics, with the lowest cell viability exceeding 93.96% of the control. Therefore, it was concluded that the hybrid exhibited excellent biocompatibility. Additionally, alkaline phosphatase (ALP) activity testing using rat bone mesenchymal stem cells (rBMSCs) as shown in Figure 5c, with Control representing the culture medium and OT representing the osteogenic medium, compared the 60S/40G hybrid with the inclusion of both antibiotics. It was evident that the hybrid demonstrated favorable ALP activity. Turner et al.[34] conducted a quantitative review of Si species released on cell behavior, revealing that Si at concentrations of 15–50 ppm can increase cell metabolic activity and enhance the proliferation of osteoblasts. As the concentration of released Si increases to 160 ppm, it can further assist in the proliferation of human osteoblasts and new bone formation. Due to the ability of Si ions to react with different elements in the human body such as Ca, P, and Na, creating a microenvironment preferred by cells, thus ALP activity increases.[35]

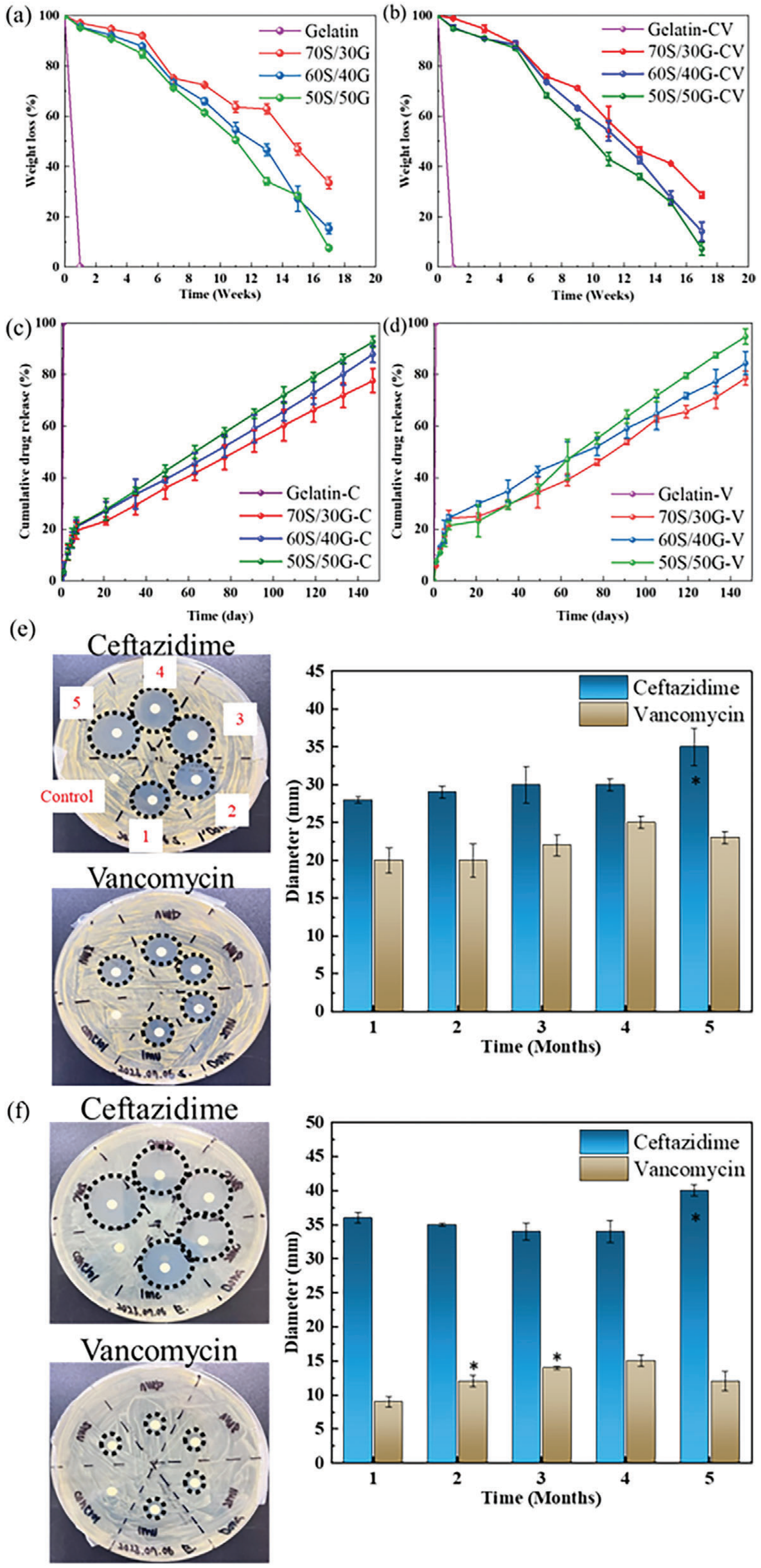

Figure 4. Illustrates the degradation patterns of Gelatin, 70S/30G, 60S/40G, and 50S/50G: a) with and b) without antibiotics. Additionally, c) displays the cumulative drug release of Gelatin, 70S/30G, 60S/40G, and 50S/50G with Ceftazidime, while d) presents the release with Vancomycin antibiotics. The antibacterial efficacy was assessed through e) tests against *Staphylococcus aureus* (*S. aureus*) and f) samples tested against *Escherichia coli* (*E. coli*), accompanied by optical images showing the zone of inhibition. (Red numbers 1, 2, 3, 4, and 5 represent the months in which the same arrangement occurs in all samples.) * indicates $p < 0.05$.

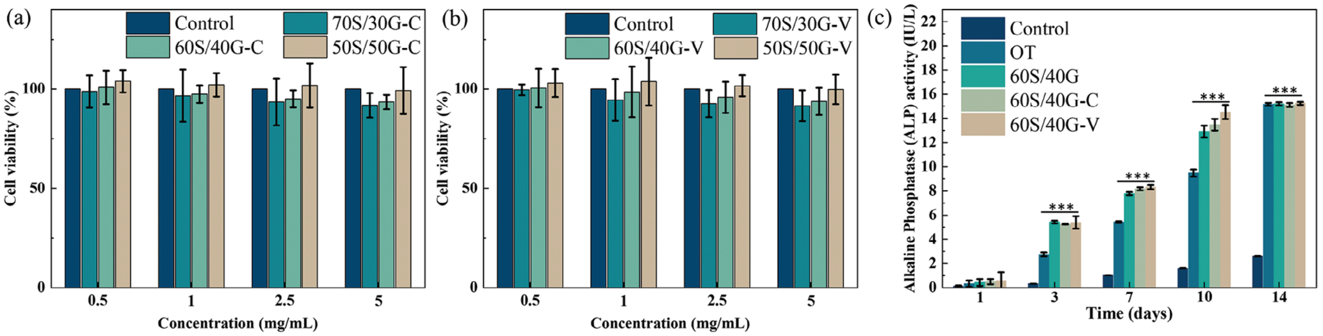

Figure 5. a) The CCK-8 test measures the viability of rBMSCs on gelatin, 70S/30G, 60S/40G, and 50S/50G with Ceftazidime, and b) The CCK-8 test measures the viability of rBMSCs on gelatin, 70S/30G, 60S/40G, and 50S/50G with Vancomycin co-cultured with L929 fibroblasts. c) displays the rBMSCs ALP activity test results for 60S/40G, 60S/40G-C, and 60S/40GV over 1, 3, 7, 10, and 14 days. The control represents the culture medium, and OT represents the osteogenic medium. *** indicates $p < 0.001$.

2.5. In Vitro Wound Healing Assay and Hemolysis Test

Compared to traditional antibiotic-loaded PMMA beads, gelatin–silica hybrid has demonstrated excellent and homogeneous degradation properties. However, as the hybrid serves as a drug carrier, it also occupies the position of the wound. Therefore, the material's role in wound healing is crucial. This study utilized an in vitro wound healing assay to simulate cell migration for bridging and repairing, and to monitor the healing process.[36] The microscopic results of co-culturing the material with L929 cells for 24 h are presented in **Figure 6**a. In Figure 6b, the changes in the wound area were statistically analyzed. At 3 h, hybrids with added antibiotics exhibited a significant wound healing effect, with the 60S/40G hybrid showing better wound healing than the medium alone. Previous research has suggested that adding tobramycin antibiotics to hydrogels may induce endoplasmic reticulum stress in cells, promoting cell migration.[37] Alternatively, different antibiotic concentrations may stimulate immune cell migration, achieving a defensive effect against infection. Ceftazidime, in particular, has a direct positive effect on granulocyte-stimulated migration.[38]

The hemolysis rate is crucial for assessing the biocompatibility of implanted biomedical materials. According to ASTM F756 Standard Practice for Assessment of Hemolytic Properties of Materials, a hemolysis rate and hemolysis index below 2% can be defined as non-hemolytic. Figure 6c,d illustrates the hemolytic properties of the material. It is evident that rat blood exhibits complete hemolysis in a DI water environment. However, the hybrid material consistently demonstrates hemolysis rates below 0.5% and hemolytic indices below 1% under any conditions. Therefore, the hybrid material exhibits excellent biocompatibility regardless of the presence of antibiotics.

2.6. In Vivo Studies and Bone Defect Observation

Figure 7 presents the hematoxylin and eosin (H&E)-stained histological section analysis of the cranial defect experiment. The hybrid material is well-integrated with surrounding tissues, showing no distinct interface and indicating excellent biocompatibility. Only a slight inflammatory reaction is observed. Partial new bone regeneration and vascular formation are seen 3 weeks post-surgery. By 13 weeks, new bone formation is evident along the material boundaries, with noticeable material degradation. The 60S/40G-C sample shows significant immune cell accumulation. **Figure 8** shows the Masson's trichrome staining results. At 3 weeks, all samples exhibit new blood vessel formation and collagen fiber growth. By 13 weeks, significant muscle fiber formation is observed, with the 60S/40G-C sample displaying higher cell nucleus density. Previous studies indicate that some antibiotics may affect the immune response, with Ceftazidime enhancing immunoregulatory functions such as chemotaxis and phagocytosis, while Vancomycin has minimal impact.[39]

Figure 9 presents computed tomography (CT) scan results of cranial defects in Sprague Dawley (SD) rats at 1, 3, 9, and 13 weeks, showing bone defect healing. **Table 1** lists the areas of bone defect repair. During the first three weeks of wound healing, 60S/40G samples exhibited better bone repair effects. Over time, at 13 weeks, the untreated control group showed 40.1 ± 2.7% bone healing, compared to 43.7 ± 0.8% for 60S/40G, 38.8 ± 2.2% for 60S/40G-C, and 32.8 ± 1.8% for 60S/40G-V. Previous studies have suggested that antibiotics play a role in infection resistance, and through the synergistic action of the immune system, antibiotics stimulate the release of cytokines and growth factors. This leads to a positive cascade effect that recruits additional cells and stimulates the migration of mesenchymal stem cells for wound repair.[40] However, research on sustained and high-concentration antibiotic-release carriers is limited. It is widely believed that prolonged and high-concentration antibiotics can impact bone and bone healing. Garza et al. suggest that the inflammatory cytokine IL-1β and keratinocyte-dependent IL-1R-MyD88 signaling are necessary and sufficient for bacteria to promote regeneration, and complete elimination of bacteria is unfavorable for wound repair.[41] In Giannoudis et al.'s review article, contradictory results were found in 17 in vivo studies on antibiotics and bone healing.[42] The major consensus is that high concentrations of antibiotics may inhibit osteoblast proliferation,[43] and in higher concentrations, cell apoptosis may occur. The most controversial point is the concentration of antibiotic use, but in clinical practice, the removal of infection risk is considered a priority over slowing bone tissue healing.

Blood parameters, including GOT, GPT, BUN, and CRE, were measured and are presented in **Table 2**.[44] GOT, GPT, and BUN indices are associated with damage to vital organs such

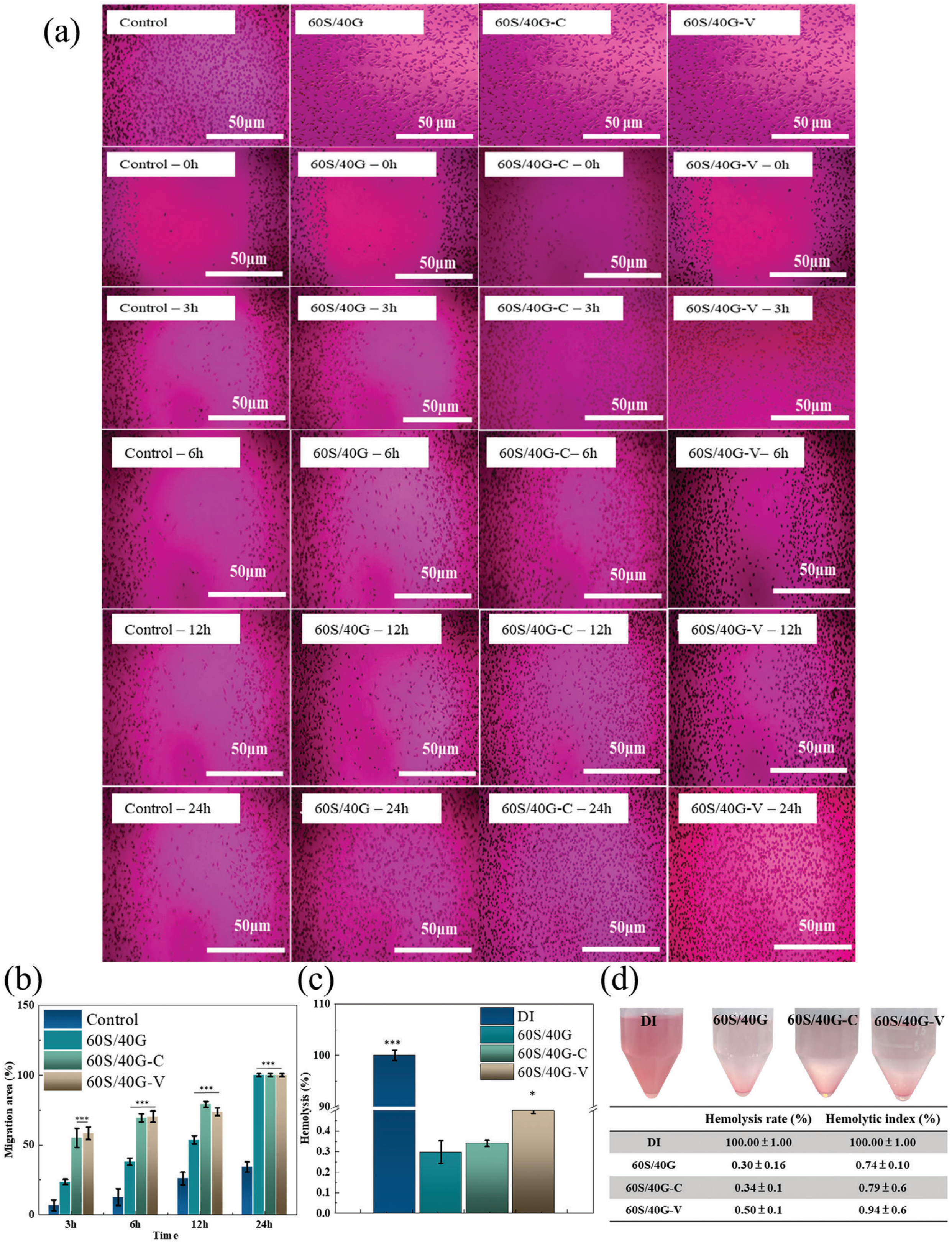

	Hemolysis rate (%)	Hemolytic index (%)
DI	100.00 ± 1.00	100.00 ± 1.00
60S/40G	0.30 ± 0.16	0.74 ± 0.10
60S/40G-C	0.34 ± 0.1	0.79 ± 0.6
60S/40G-V	0.50 ± 0.1	0.94 ± 0.6

Figure 6. a) Wound healing assay to evaluate the cell migration rate on the material for 24 h; b) the trend bar chart of cell migration area; c) hemolysis of the materials; d) the optical images of the hemolysis test and the lists of hemolysis rate and hemolytic index for DI water, 60S/40G, 60S/40G-C, and 60S/40G-V, respectively. * and *** indicate $p < 0.05$ and $p < 0.001$.

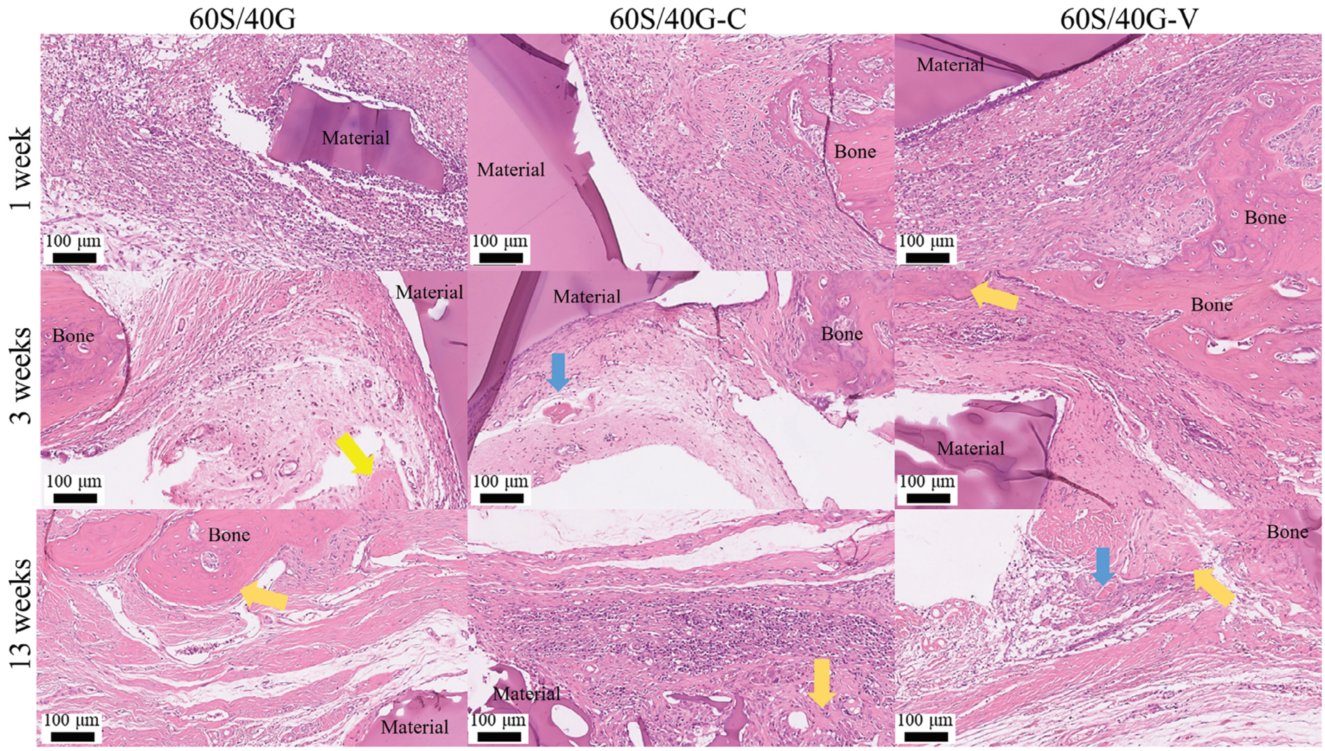

Figure 7. H&E staining of 60S/40G, 60S/40G-C, and 60S/40G-V applied on cranial defect for 1, 3, and 13 weeks. Blue arrows indicate the inflammation area, while yellow arrows indicate the new bone regeneration area. The scale bars are 100 µm.

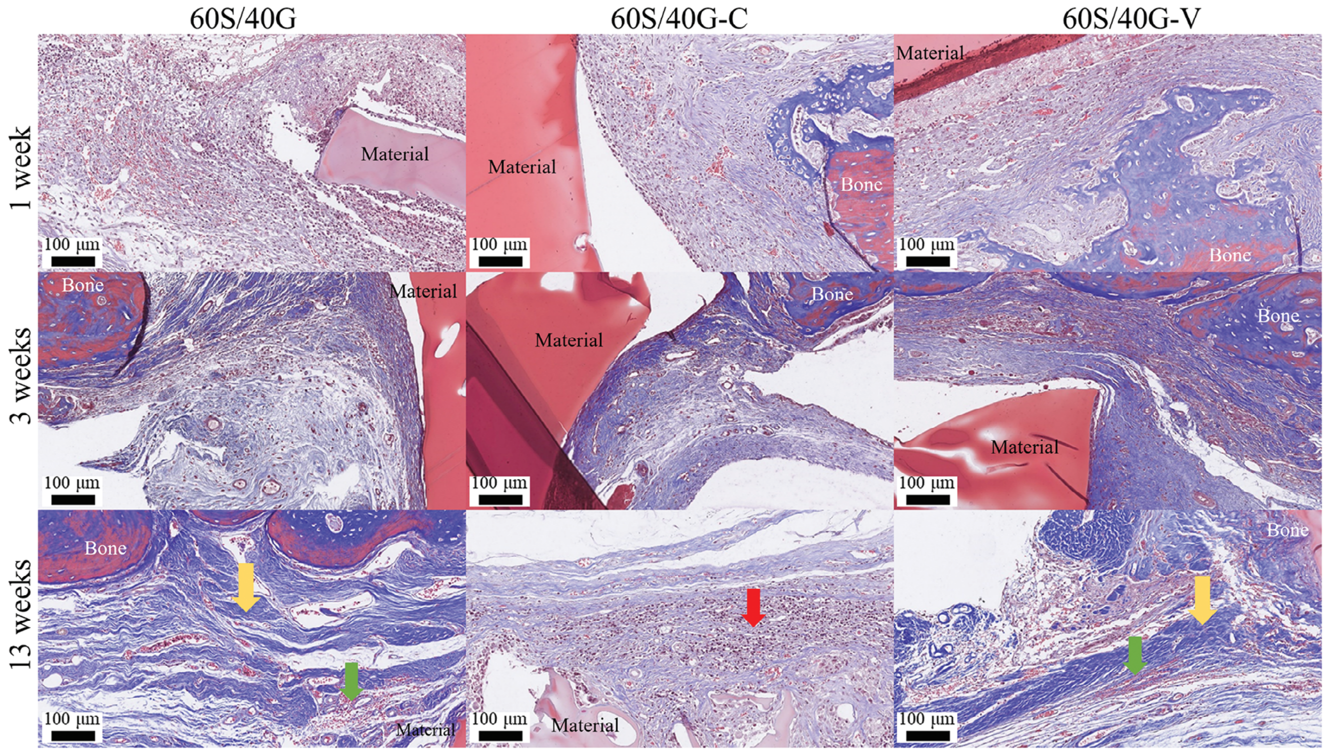

Figure 8. Masson's trichrome staining of 60S/40G, 60S/40G-C, and 60S/40G-V applied on cranial defect for 1, 3, and 13 weeks. Green arrows indicate muscle fibers, yellow arrows indicate collagen fibers and the red arrow indicates cell nuclei. The scale bars are 100 µm.

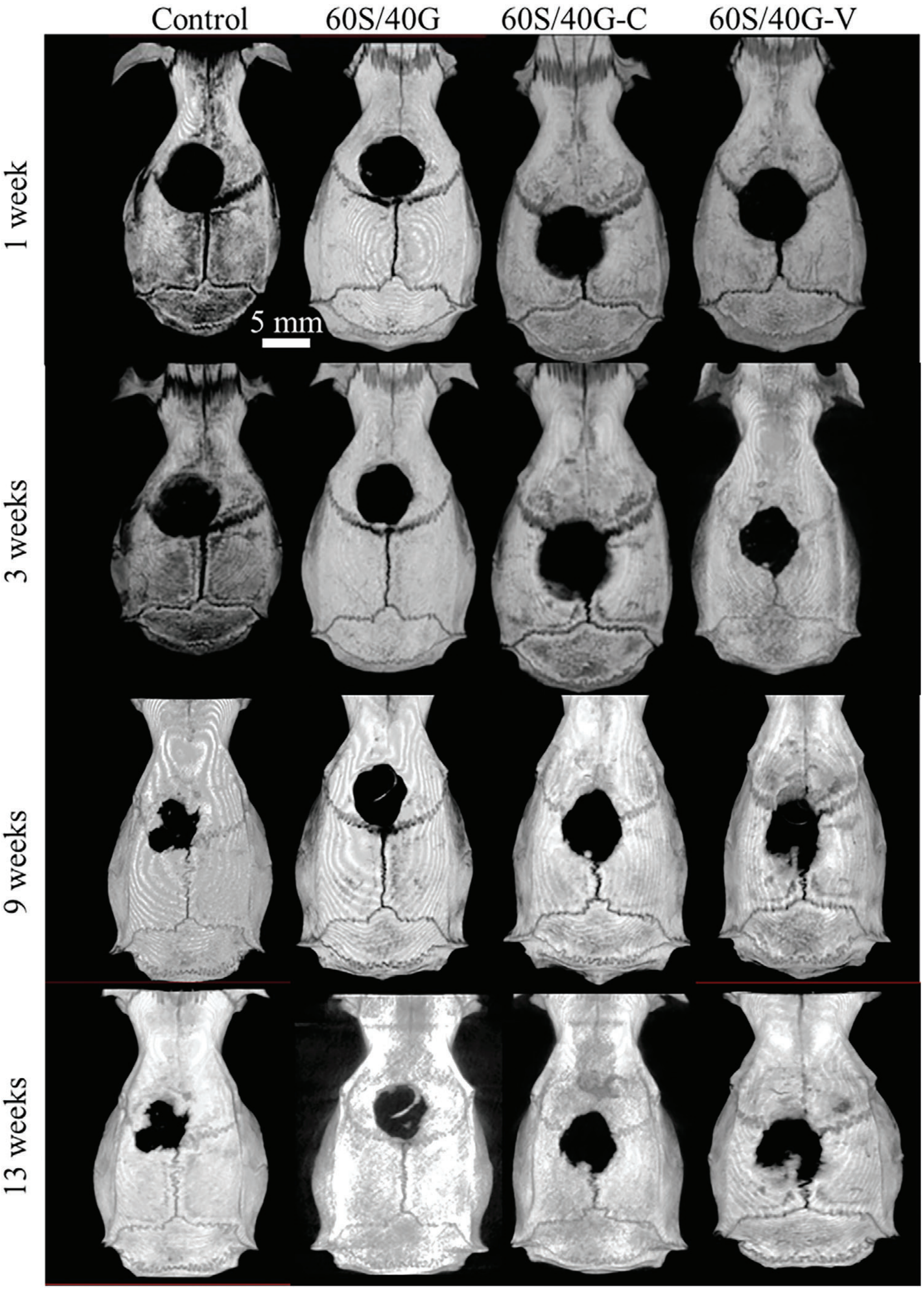

Figure 9. CT images of cranial defect repair through the implantation of 60S/40G, 60S/40G-C, and 60S/40G-V to aid in defect repair. CT images were used to observe the new bone formation and defect healing at 1, 3, 9, and 13 weeks after the implantation of materials.

Table 1. The list of bone defect healing areas at 1, 3, 9, and 13 weeks determined through CT images; healing areas were calculated using ImageJ.

Samples	Control	60S/40G	60S/40G-C	60S/40G-V
1 week	5.4 ± 1.9%	10.4 ± 1.8%	14.7 ± 1.8%	11.3 ± 1.9%
3 weeks	8.2 ± 1.9%	19.9 ± 0.7%	23.6 ± 2.7%	15.4 ± 1.3%
9 weeks	35.8 ± 2.3%	34.0 ± 0.5%	32.4 ± 3.0%	24.5 ± 1.5%
13 weeks	40.1 ± 2.7%	43.7 ± 0.8%	38.8 ± 2.2%	32.8 ± 1.8%

as the heart, liver, and kidneys. The distribution of GOT and GPT values did not indicate significant damage in the mean values.[45] However, in the 13-week experiment, the BUN indices of the 60S/40G-C and 60S/40G-V groups were slightly higher compared to the control and 60S/40G hybrid groups, possibly due to the increased renal load caused by prolonged antibiotic release. Nevertheless, these values remained within the reference range. On the other hand, the CRE values in all groups consistently fell below the reference range. Since CRE is an

Table 2. Serum levels of AST (GOT), GPT (ALT), BUN, and CRE in SD rats after the implantation of hybrid materials. Reference ranges are based on literature.[44] The full names of the indicators are as follows: AST: Aspartate Aminotransferase (also known as GOT: Glutamic-Oxaloacetic Transaminase), ALT: Alanine Aminotransferase (also known as GPT: Glutamic-Pyruvic Transaminase), BUN: Blood Urea Nitrogen, CRE: Creatinine.

	Sample	AST/GOT [U/l]	ALT/GPT [U/l]	BUN [mg/dl]	CRE [mg/dl]
Week 1	Control	122.00 ± 8.48	50.50 ± 12.02	28.85 ± 3.46	0.28 ± 0.05
	60S/40G	88.00 ± 5.65	30.50 ± 0.71	19.25 ± 0.07	0.29 ± 0.01
	60S/40G-C	169.11 ± 19.79	43.54 ± 2.12	17.20 ± 0.98	0.25 ± 0.06
	60S/40G-V	104.72 ± 7.12	43.33 ± 15.55	19.15 ± 4.45	0.27 ± 0.01
Reference range	37–205	6–114	13–29	0.4–1.5	
Week 13	Control	96.00 ± 11.31	41.00 ± 7.07	17.65 ± 0.07	0.29 ± 0.01
	60S/40G	126.50 ± 17.67	42.00 ± 7.07	17.45 ± 0.07	0.24 ± 0.01
	60S/40G-C	129.41 ± 66.46	42.35 ± 7.07	21.65 ± 6.01	0.28 ± 0.02
	60S/40G-V	135.00 ± 72.12	40.50 ± 6.36	21.15 ± 0.49	0.23 ± 0.00
Reference range	37–205	6–114	13–29	0.4–1.5	

indicator of muscle metabolism, the lower values may be attributed to a decrease in muscle mass resulting from reduced physical activity post-surgery, ultimately leading to lower CRE levels throughout the experiment.[46] This study successfully prepared a controllable and homogeneous gelatin–silica hybrid for controlled degradation and antibiotic release. However, prolonged high-concentration antibiotic release may slow bone growth. In practical applications, infection elimination is prioritized, so antibiotic concentration should be adjusted as needed. Future research on sustained antibiotic release for bone regeneration is essential.

3. Conclusion

Taken together, a biodegradable and uniformly degradable antibiotic carrier has been successfully developed. The gelatin–silica hybrid functions as an effective degradable antibiotic carrier, exhibiting exceptional operability. By adjusting the silica content, both mechanical properties and degradation rate can be managed. Additionally, the hybrid permits the incorporation of high antibiotic concentrations, up to 10 wt%, without compromising its mechanical integrity, demonstrating consistent degradation and drug release characteristics. Even after 5 months of antibiotic release, it retains effective antibacterial properties. While in vivo experiments indicate a slight reduction in bone healing efficiency for hybrids containing antibiotics compared to those without, they ensure infection risk elimination without significant harm to vital organs.

4. Experimental Section

Materials: Gelatin powder from porcine skin (Type A, gel strength ≈300 g Bloom), L-Ascorbic acid, Cell Counting Kit-8 (CCK-8), and Sodium sulfate (Na_2SO_4) were purchased from Sigma Aldrich, USA. Tris (Base), Sodium Bicarbonate ($NaHCO_3$), Calcium Chloride ($CaCl_2$), Magnesium phosphate,6-hydrate ($MgCl_2 \cdot 6H_2O$), Potassium Chloride (KCl), Sodium Chloride (NaCl), and Dipotassium phosphate (K_2HPO_4) were purchased from J.T Baker/USA. 3-Glycidoxypropyltrimethoxysilance, 97% (GPTMS), Tetraethyl orthosilicate (TEOS), and hydrogen chloride (HCl) were purchased from Jingming Chemicals, Taiwan. Minimum Essential Medium (Alpha Medium) and Dulbecco's Modified Eagle Medium (DMEM) were purchased from Invitrogen, USA. MEM-non-essential amino acid, 5% Trypsin-EDTA, and Penicillin-Streptomycin (PS) were purchased from Gibco, USA. Hydrogen Chloride (HCl) was purchased from Hanawa, Japan. Fetal Bovine Serum (FBS) was purchased from Biological Industries/Israel. ß-Glycerphosphoric acid was purchased from ACROS/Belgium. Sodium Phosphate Dibasic Dihydrate ($NaHPO_4 \cdot 2H_2O$) was purchased from Riedel-de Haën, Germany.

Preparation of Gelatin and Silica Hybrid: Organic and inorganic (gelatin-silica) hybrids were synthesized by controlling the ratios between gelatin and TEOS precursors. Three different ratios of gelatin were prepared by dissolving gelatin in distilled water at 40 °C. The solution was stirred continuously at 400 rpm until completely dissolved. Then, GPTMS was added to the gelatin solution and stirred for 30 min for ring-opening and amino-epoxy reaction.[21] The concentrations of reagents were listed in **Table 3**.

In another beaker, TEOS was hydrolyzed by adding DI water and 1 M HCl to the TEOS solution, and the mixture was allowed to hydrolyze for at least 1 h. Subsequently, hydrolyzed TEOS solutions were mixed into the gelatin solution. The mixtures gelled after 10–20 min, with higher silica concentration resulting in a shorter gelation time than the low silica concentration sample. Meanwhile, samples were shaped by hand or using a 15 mm diameter and 30 mm height Teflon mold and dried at room temperature for further mechanical tests.

During the gelation process, antibiotic-loaded gelatin–silica hybrids were prepared. Specifically, 10 wt% of Vancomycin hydrochloride and/or Ceftazidime antibiotic powders were directly mixed into the mixture immediately after the hydrolyzed TEOS solution was added to the gelatin solution. These antibiotics were evenly added and mixed during the solidification period. However, the gelation time decreased by ≈5–15 min with the addition of more antibiotics, finally following the same shaping method as mentioned above.

Characterization of the Scaffold: To identify the functional groups and molecular interactions in the scaffold, the samples were cut into 1 mm × 1 mm, and attenuated total reflection-Fourier-transform infrared spectroscopy (ATR-FTIR, Spotlight 200i Sp2 with AutoATR System, Perkin

Table 3. Precursor concentrations of gelatin–silica hybrid.

Composition [Silica/Gelatin, wt%]	70S/30G	60S/40G	50S/50G
Gelatin	1.97 g	3.07 g	4.61 g
DI Water	6.1 mL	8.27 mL	11.34 mL
GPTMS	0.26 mL	0.26 mL	0.26 mL
TEOS	5.04 mL	5.04 mL	5.04 mL
1 M HCl	0.71 mL	0.71 mL	0.71 mL

Elmer, USA) analysis was performed with a measuring range of 4000–500 cm^{-1}. Similarly, ^1H nuclear magnetic resonance (NMR, 400 MHz Spectrometer, JEOL, Japan) was also conducted to detect changes in the chemical structure. Samples were dissolved in $CDCl_3$ to achieve a final concentration of 10 mg mL^{-1} for NMR analysis. Gelatin–silica hybrid samples were collected after mixing hydrolyzed TEOS into gelatin solution. It takes ≈10–20 min for the mixture to solidify, so the samples were dissolved in $CDCl_3$ while in a semi-gelled state. To analyze the individual weight percentage of organic and inorganic compounds, thermogravimetric analysis (TGA, STA7300, HITACHI, Japan) was performed. The surface morphology and microstructure of the scaffold were investigated by scanning electron microscopy (SEM), and their elemental composition was analyzed by energy-dispersive X-ray spectroscopy (EDX, S-3000H, Hitachi, Japan) after sputtering the samples with Au. The mechanical properties of the scaffold were tested using a universal testing machine (UTM, Junyan Precision Machinery Co., Ltd., Taiwan). For the compression test, stainless steel platforms were used to place cylindrical-shaped samples measuring 15 mm × 30 mm, and they were loaded with a compression rate of 0.5 mm^{-1} sec.

Swelling and Degradation Tests: For the swelling tests, the samples were cut into sheets with dimensions of 10 mm × 10 mm × 1 mm, and their dry weight was measured (W0). Subsequently, the scaffolds were soaked in 20 mL of phosphate-buffered saline (PBS, pH 7.0) at 37 °C. At various time points, the samples were removed, and their weights (W) were measured. The swelling ratio (SR) was calculated using Equation (1).

$$SR = \frac{W - W_0}{W_0} \tag{1}$$

For degradation tests, the samples were cut into sheets with dimensions of 10 mm × 10 mm × 1 mm and freeze-dried. The initial dry weight (W0) of the samples was measured. The samples were then incubated in PBS (pH 7.0), PBS with 0.5 mg mL^{-1} lysozyme, and PBS without lysozyme at 37 °C for 17 weeks and 9 weeks, respectively. At different time points, the samples were removed and lyophilized to measure the remaining weight (Ww). The degradation rate of the samples was calculated using Equation (2).

$$\text{Weight loss } (\%) = \frac{W_0 - W_W}{W_0} \text{ X } 100\% \tag{2}$$

Drug Release: The standard drug release concentrations were calibrated using a UV–vis Spectrophotometer (UV–vis, SP-8001, Yoyu/Taiwan). Vancomycin and Ceftazidime were dissolved in PBS (pH 7.0) at 37 °C, with concentrations ranging from 1 mg mL^{-1} to 1 ng mL^{-1}.

10 mg of gelatin–silica hybrid were soaked in 10 mL of PBS with and without 0.5 mg mL^{-1} lysozyme at 37 °C for 17 weeks and 9 weeks. At various time points, 5 mL of the solution was replaced with fresh PBS to measure the drug release concentration.

Antibacterial Test: The antibacterial activity of the samples was evaluated by a zone of inhibition test. For this test, *S. aureus* and *E. coli* strains were used. A 1 mL suspension of 1×10^6 CFU mL^{-1} bacteria was spread onto a 150 mm diameter agar plate. A 6 mm diameter antibiotic paper tablet containing 25 µL of the drug-released test solution, or PBS as a control, was placed on the plate and incubated at 37 °C for 24 h. The antibacterial effect was assessed by observing the size of the antibacterial zone on the agar plate.

Cell Viability Test: The cells used in this study were mouse fibroblasts (L929), human osteosarcoma cells (MG63), and rat bone marrow mesenchymal stem cells (rBMSCs). Cells were cultured with DMEM supplemented with 10% Fetal Bovine Serum (FBS), 1% penicillin/streptomycin, and incubated at 37 °C with 5% CO_2. Cytotoxicity of L929 and rBMSCs on gelatin–silica hybrid samples were evaluated using the cell counting kit (CCK-8) technique.

In brief, different concentrations of gelatin–silica hybrid samples (0.5, 1, 2.5, and 5 mg mL^{-1}) were incubated in DMEM at 37 °C for 24 h. After that, the scaffold was filtered, taken out, and seeded with 1×10^4 cells in a 96-well plate with as-prepared DMEM and incubated in a humidified incubator at 37 °C with 5% CO_2 for 1 day. After 1 day, CCK-8 reagent was added to each well and incubated for 1 h. Finally, absorbance was measured at a wavelength of 450 nm. Cell viability (%) was calculated using Equation (3).

$$\text{Cell viability } (\%) = \frac{(Absorbance\ of\ experimental\ group - Absorbance\ of\ blank)}{(Absorbance\ of\ control - Absorbance\ of\ blank)} \times 100\% \tag{3}$$

Alkaline Phosphatase Activity: To investigate the osteogenic property of the gelatin–silica hybrid scaffolds, alkaline phosphatase (ALP) activity was measured. Initially, 1×10^4 cells were seeded in a 24-well plate and incubated at 37 °C with 5% CO_2. To prepare the osteogenic culture medium, 10 mм β-glycerophosphate, 0.2 mм ascorbic acid, and 0.1 mм dexamethasone were added to DMEM, which contains a 5 mg mL^{-1} gelatin–silica hybrid scaffold. After 24 h, the original culture medium was removed from the 24-well plate, washed with PBS, and 500 µL of osteogenic medium was added to each well, followed by incubation at 37 °C in a CO_2 incubator for 1, 3, 7, 10, and 14 days. The culture medium was changed every 3 days during this time. At each specific time point, the medium was removed from each well, washed with PBS, and 500 µL of 0.2% Triton X-100 was added, with the plates kept at room temperature for 20 min. Then, a reagent solution containing Assay buffer (200 µL), Magnesium acetate (0.2 м, 5 µL), and pNpp liquid (1 м, 2 µL) was added to the well. Finally, the absorbance values at 0 and 4 min at a wavelength of 405 nm were measured. The ALP activity was calculated using Equation (4).

$$ALP\ activity = \frac{(OD_T - OD_{To}) \times 1000\ \times V_{final}}{\epsilon PNP\ \times L\ \times V_{sample}\ \times\ T} \tag{4}$$

where the OD was optical density, T was reaction time, T_0 was time 0, V_{final} was final reaction volume, ϵPNP represents the molar absorptivity of p-nitrophenol (18.75 $mм^{-1} \times cm^{-1}$), L represents the optical path length in mm, and V_{sample} was the sample volume.

Cell Migration Assay: For the cell migration assay, the gelatin–silica hybrid scaffolds were placed in serum-free or less than 2% DMEM to achieve a final concentration of 0.5 mg mL^{-1} and incubated at 37 °C for 24 h. In 6-well plates, three horizontal lines were drawn with a spacing of 0.5–1 cm. Each well was seeded with 5×10^5 cells and the cells were dispersed evenly. Using a 1000 µL tip, a scratch was made vertically in the well plate, along with a vertical cut following the marked line when the cell density reached 90%. The culture medium was removed, the wells were washed with PBS, and culture medium with gelatin–silica hybrid samples at a concentration of 0.5 mg mL^{-1} was added. The plate was then placed at 37 °C in a 5% CO_2 incubator. At 0, 3, 6, 12, and 24 h, pictures were taken using an optical microscope to observe the cell migration speed. Using Image J software, the migration area was calculated.

Hemolysis Assay: The hemolysis test was performed following the ASTM F756 (2000) standard. In brief, mix hemoglobin standard with Drabkin's reagent (Sigma–Aldrich, USA) to obtain a concentration of 1000 µg mL^{-1}. Dilute the mixture to concentrations of 800, 600, 400, 200, 100, and 50 µg mL^{-1}. Take 1 mL from each dilution and measure the absorbance at a wavelength of 540 nm using a UV spectrophotometer. Calculate the standard curve based on these absorbance values.

In this experiment, Sprague–Dawley (SD) rat blood was used. After diluting the blood and comparing it with the standard curve, hemolysis experiments were conducted with a PBS concentration adjusted to 25 mg mL^{-1}. After pre-swelling a 1 cm^2 hybrid in PBS for 1 h, place it in a 15 mL centrifuge tube and add 5 mL of the adjusted blood sample. Mix and incubate in a 37 °C incubator for 4 h. Take 1 mL for centrifugation, and after centrifugation, measure the absorbance to calculate the concentration.

The hemolysis ratio and index were calculated using Equations (5) and (6).

$$Hemolysis\ Ratio\ (\%) = \frac{OD_{sample} - OD_{neg.}}{OD_{pos.} - OD_{neg.}} \times 100\% \quad (5)$$

$$Hemolysis\ Index\ (H.I,\ \%) = \frac{OD_{sample}}{OD_{pos.}} \times 100\% \quad (6)$$

Finally, the OD values obtained from the treated samples (ODsample) were normalized relative to the positive control (100% lysis; ODpos) and negative control (untreated; ODneg) samples.[47]

Animal Test: This in vivo experiment was conducted at Chang Gung Memorial Hospital, Linkou, Taiwan (IACUC2023030305), using 6-week-old Sprague Dawley (SD) rats. The rats were divided into two groups: the control group containing gelatin–silica hybrid (60S/40G) and the experimental group comprising 60S/40G containing 10 wt% Ceftazidime (60S/40G-C) and 60S/40G containing 10 wt% Vancomycin hydrochloride (60S/40G-V). In summary, Zoletil 50 and Rompun 20 were mixed in a 1:2 ratio to prepare an anesthetic solution, administered at 0.1 mL of anesthetic solution per 100 g of rat weight through intraperitoneal injection. A 5 mm skull defect was created using a microdrill. Samples were prepared and shaped as 5 mm in diameter and 2 mm in height, fitting into the skull defect. Absorbable sutures were used to close the wound. Skull repair progress was observed on days 1, 3, 9, and 13 weeks after surgery, and computer tomography (CT) was used to monitor the skull repair area. Finally, euthanasia was performed using CO_2, and the skull defect was taken and fixed in formalin. H&E and Masson staining procedures were conducted by Toson Technology Co. Ltd. in Taiwan. Subsequently, scanning images were utilized to analyze the stained samples.

Biochemical tests, assessing renal function through blood urea nitrogen (BUN) and creatinine (CRE), as well as liver function through glutamic oxaloacetic transaminase (GOT) and glutamic pyruvic transaminase (GPT), were conducted to evaluate the impact of the test materials on visceral function. Subsequently, animals were euthanized using carbon dioxide, and tissue sections were obtained for staining, including Hematoxylin and Eosin (H&E) and Masson's trichrome staining.

Statical Analysis: The collected results data in this study were subjected to statistical analysis using Origin software. Group differences in numerical values were compared using the Tukey test. All experiments followed a completely random design. When the data exhibited significant differences, it was denoted as $^{*}p < 0.05$, highly significant differences as $^{**}p < 0.01$, and very highly significant differences as $^{***}p < 0.001$. When the differences between two sets of data were not significant, it was indicated as $p > 0.05$.

Supporting Information

Supporting Information is available from the Wiley Online Library or from the author.

Acknowledgements

Technical assistance from the Precision Analysis and Material Research Center of the National Taipei University of Technology (Taipei Tech) is appreciated. The authors are grateful for the financial support received from the National Science and Technology Council of Taiwan (NSTC 111-2622-E-027-022; NSTC 112-2622-E-027-020; NSTC 112-2314-B-182A-102-MY2). In addition, this work was financially supported by the Tier 3 program (grant no. MOET32022-0008). The authors also thank their colleagues in the Translational Materials Innovation Group (TMIG) and the Centre for Cross Economy.

Conflict of Interest

The authors declare no conflict of interest.

Data Availability Statement

The data that support the findings of this study are available from the corresponding author upon reasonable request.

Keywords

antibacterial activity, biodegradable, bone filler, gelatin–silica hybrid, long-term antibiotic release

Received: June 1, 2024
Revised: August 1, 2024
Published online:

---

[1] Z. Li, Y. Zhao, Z. Wang, M. Ren, X. Wang, H. Liu, Q. Lin, J. Wang, *Adv. Healthcare Mater.* **2022**, *11*, 2102535.
[2] C. Hamad, M. Chowdhry, D. Sindeldecker, N. M. Bernthal, P. Stoodley, E. J. McPherson, *Bone Joint J.* **2022**, *104*, 575.
[3] S. M. Kurtz, E. C. Lau, M.-S. Son, E. T. Chang, W. Zimmerli, J. Parvizi, *J. Arthroplasty* **2018**, *33*, 3238.
[4] a) S. M. Kurtz, K. L. Ong, J. Schmier, F. Mowat, K. Saleh, E. Dybvik, J. Kärrholm, G. Garellick, L. I. Havelin, O. Furnes, *JBJS* **2007**, *89*, 780; b) A. Premkumar, D. A. Kolin, K. X. Farley, J. M. Wilson, A. S. McLawhorn, M. B. Cross, P. K. Sculco, *J. Arthroplasty* **2021**, *36*, 1484.
[5] K. Jie, P. Deng, H. Cao, W. Feng, J. Chen, Y. Zeng, *PLoS One* **2019**, *14*, e0223402.
[6] F. Iannotti, P. Prati, A. Fidanza, R. Iorio, A. Ferretti, D. Pèrez Prieto, N. Kort, B. Violante, G. Pipino, A. Schiavone Panni, *Trop. Med. Infect. Dis.* **2020**, *5*, 186.
[7] T. A. Van Vugt, J. J. Arts, J. A. Geurts, *Front. Microbiol.* **2019**, *10*, 451409.
[8] D. M. Janssen, P. Willems, J. Geurts, C. J. Arts, *J. Orthop. Res.* **2023**, *41*, 1831.
[9] A. C. Dibartola, M. C. Swearingen, J. F. Granger, P. Stoodley, D. H. Dusane, *APMIS* **2017**, *125*, 418.
[10] Y.-H. Hsu, C. Hu, P.-H. Hsieh, H.-N. Shih, S. W. Ueng, Y. Chang, *JBJS* **2017**, *99*, 223.
[11] W. Steadman, P. R. Chapman, M. Schuetz, B. Schmutz, A. Trampuz, K. Tetsworth, *Antibiotics* **2023**, *12*, 752.
[12] J. N. Insall, F. M. Thompson, B. D. Brause, *JBJS* **2002**, *84*, 490.
[13] D. M. Janssen, J. A. Geurts, L. M. Jütten, G. H. Walenkamp, *Acta Orthop.* **2016**, *87*, 324.
[14] Y.-C. Lin, H.-Y. Wang, Y.-C. Tang, W.-R. Lin, C.-L. Tseng, C.-C. Hu, R.-J. Chung, *Int. J. Biol. Macromol.* **2023**, *258*, 128845.
[15] O. Mahony, O. Tsigkou, C. Ionescu, C. Minelli, L. Ling, R. Hanly, M. E. Smith, M. M. Stevens, J. R. Jones, *Adv. Funct. Mater.* **2010**, *20*, 3835.
[16] A. Negahi Shirazi, A. Fathi, F. G. Suarez, Y. Wang, P. K. Maitz, F. Dehghani, *ACS Appl. Mater. Interfaces* **2016**, *8*, 1676.
[17] a) N. Sahai, M. Anseau, *Biomaterials* **2005**, *26*, 5763; b) O. Mahony, S. Yue, C. Turdean-Ionescu, J. V. Hanna, M. E. Smith, P. D. Lee, J. R. Jones, *J. Sol-Gel Sci. Technol.* **2014**, *69*, 288.
[18] a) H. Yu, J. Peng, Y. Xu, J. Chang, H. Li, *ACS Appl. Mater. Interfaces* **2016**, *8*, 703; b) F. Tallia, L. Russo, S. Li, A. L. Orrin, X. Shi, S. Chen, J. A. Steele, S. Meille, J. Chevalier, P. D. Lee, *Mater. Horiz.* **2018**, *5*, 849.
[19] R. Ellerbrock, M. Stein, J. Schaller, *Sci. Rep.* **2022**, *12*, 11708.

[20] Y.-C. Lin, E. J. Nixon, H.-Y. Wang, U. Dhawan, Y.-W. Huang, S.-H. Huang, C.-P. Jiang, Y.-J. Kuo, R.-J. Chung, *ACS Appl. Polym. Mater.* **2023**, *5*, 6012.
[21] R. Ramsdale-Capper, J. P. Foreman, *Polymer* **2018**, *146*, 321.
[22] A. S. Vega, C. Agustín-Sáenz, F. Brusciotti, A. Somers, M. Forsyth, *J. Sol-Gel Sci. Technol.* **2020**, *96*, 91.
[23] J. O. Kroll, B. J. Riley, J. S. McCloy, J. A. Peterson, *J. Sol-Gel Sci. Technol.* **2020**, *96*, 564.
[24] L. Gabrielli, L. Russo, A. Poveda, J. R. Jones, F. Nicotra, J. Jiménez-Barbero, L. Cipolla, *Chem. A Eur. J.* **2013**, *19*, 7856.
[25] L. Connell, L. Gabrielli, O. Mahony, L. Russo, L. Cipolla, J. Jones, *Polym. Chem.* **2017**, *8*, 1095.
[26] L. Gabrielli, L. Connell, L. Russo, J. Jiménez-Barbero, F. Nicotra, L. Cipolla, J. R. Jones, *RSC Adv.* **2014**, *4*, 1841.
[27] W. L. Tsang, A. C. Taylor, *J. Mater. Sci.* **2019**, *54*, 13938.
[28] J. Nam, E. Byun, H. Shim, E. Kim, S. Islam, M. Park, A. Kim, S. H. Song, *Front. Bioeng. Biotechnol.* **2020**, *8*, 596370.
[29] J. R. Jones, *Acta Biomater.* **2013**, *9*, 4457.
[30] a) A. E. Swilem, T. G. Oyama, K. Oyama, A. Kimura, M. Taguchi, *Polym. Degrad. Stab.* **2022**, *197*, 109856; b) S. P. Tsai, C. Y. Hsieh, C. Y. Hsieh, D. M. Wang, L. L. H. Huang, J. Y. Lai, H. J. Hsieh, *J. Appl. Polym. Sci.* **2007**, *105*, 1774.
[31] Y. Jang, J. Jang, B.-Y. Kim, Y.-S. Song, D. Y. Lee, *Tissue Eng. Regener. Med.* **2024**, *21*, 557.
[32] J. W. Tse, M. Rizwan, J. Rasmussen, L. Jones, E. K. Yim, *ACS Appl. Bio Mater.* **2020**, *3*, 6214.
[33] F. Morshedloo, A. B. Khoshfetrat, D. Kazemi, M. Ahmadian, *J. Biomed. Mater. Res., Part B* **2020**, *108*, 2950.
[34] J. Turner, A. Nandakumar, N. Anilbhai, A. Boccaccini, J. Jones, G. Jell, *Acta Biomater.* **2023**, *170*, 39.
[35] A. Obata, N. Iwanaga, A. Terada, G. Jell, T. Kasuga, *J. Mater. Sci.* **2017**, *52*, 8942.
[36] A. Stamm, K. Reimers, S. Strauß, P. Vogt, T. Scheper, I. Pepelanova, *BioNanomaterials* **2016**, *17*, 79.
[37] Y. Fang, T. Nie, G. Li, L. Wang, J. Du, J. Wu, *Chem. Eng. J.* **2023**, *480*, 147930.
[38] H. Gnarpe, J. Belsheim, *J. Antimicrob. Chemother.* **1981**, *8*, 71.
[39] B. Van Vlem, R. Vanholder, P. De Paepe, S. Ringoir, D. Vogelaers, *Infection* **1996**, *24*, 275.
[40] F. Shapiro, *Eur. Cell Mater.* **2008**, *15*, 53.
[41] G. Wang, E. Sweren, H. Liu, E. Wier, M. P. Alphonse, R. Chen, N. Islam, A. Li, Y. Xue, J. Chen, *Cell Host Microbe* **2021**, *29*, 777.
[42] I. Pountos, T. Georgouli, H. Bird, G. Kontakis, P. V. Giannoudis, *Expert Opin. Drug Saf.* **2011**, *10*, 935.
[43] Y. Chang, V. M. Goldberg, A. I. Caplan, *Clin. Orthop. Relat. Res.* **2006**, *452*, 242.
[44] D. M. Kurtz, G. S. Travlos, *The Clinical Chemistry of Laboratory Animals*, CRC Press, Boca Raton, Florida **2017**, 1162.
[45] a) A. Patlolla, J. Rondalph, P. Tchounwou, *Austin J. Environ. Toxicol.* **2017**, *3*, 1021; b) D. N. Che, J. Y. Shin, H. J. Kang, B. O. Cho, J. H. Park, F. Wang, S. Hao, J. S. Sim, D. J. Sim, S. I. Jang, *Food Sci. Nutr.* **2021**, *9*, 6060.
[46] A.-C. Passaquin, M. Renard, L. Kay, C. Challet, A. Mokhtarian, T. Wallimann, U. T. Ruegg, *Neuromuscul. Disord.* **2002**, *12*, 174.
[47] I. P. Sæbø, M. Bjørås, H. Franzyk, E. Helgesen, J. A. Booth, *Int. J. Mol. Sci.* **2023**, *24*, 2914.